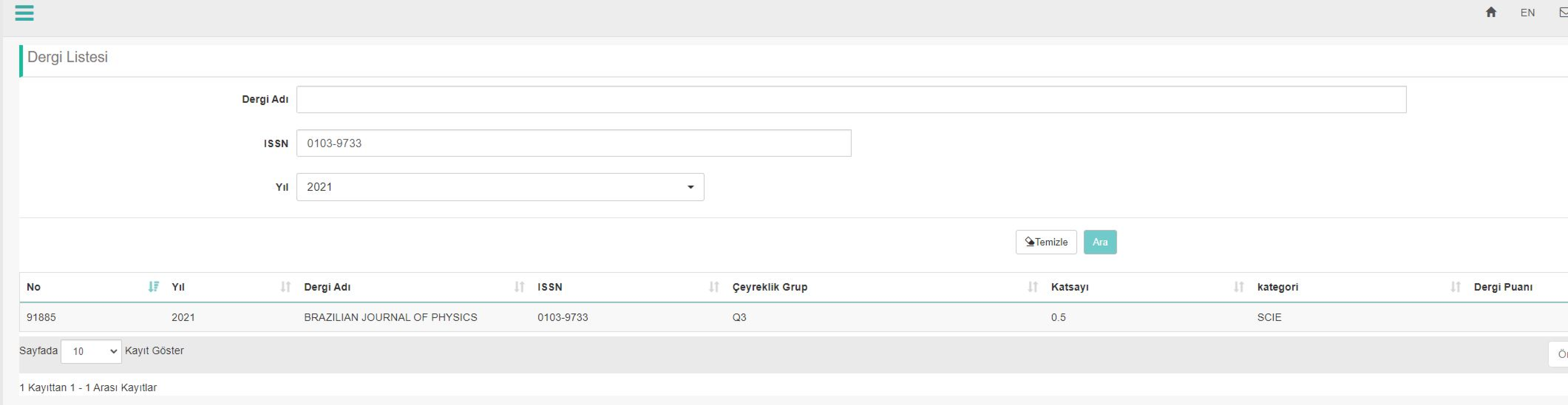

No	Yıl	Dergi Adı	ISSN	Çeyreklik Grup	Katsayı	kategori	Dergi Puanı
91885	2021	BRAZILIAN JOURNAL OF PHYSICS	0103-9733	Q3	0.5	SCIE	

Brazilian Journal of Physics (2022) 52: 184
https://doi.org/10.1007/s13538-022-01187-4

ATOMIC PHYSICS

Determination of Optical Properties of MOVPE-Grown $In_xGa_{1-x}As/InP$ Epitaxial Structures by Spectroscopic Ellipsometry

Emine Kaynar[1,2] · Muhammed Sayrac[1,2] · Ismail Altuntas[1,2] · Ilkay Demir[1,2]

Received: 1 March 2022 / Accepted: 16 August 2022 / Published online: 24 August 2022
© The Author(s) under exclusive licence to Sociedade Brasileira de Física 2022

Abstract
$In_xGa_{1-x}As$ epitaxial layers with different AsH_3 flows have been grown on InP substrate with the MOVPE system. It has been found that AsH_3 flow variation affects the In concentration of InGaAs/InP structure because the increment of AsH_3 flow increases the In concentration due to the weak bond between In and As. The variation of AsH_3 flow during the growth process has affected crystal quality and optical properties of InGaAs epilayer. The optical properties of the structure have been determined by spectroscopic ellipsometry and spectrophotometer. The variation of In concentration has changed the refractive index value of the structure. The thickness of the samples and refractive index values have been obtained by spectroscopic ellipsometry. The obtained findings show that the reflection has been improved with high AsH_3 flow resulting from surface quality improvement. In addition, it has been observed that the energy band gap has been decreased as a function of the increment of AsH_3 flow because the structure band gap approaches the InAs structure at the high In concentration.

Keywords Ellipsometry · HRXRD · Arsine flow · InGaAs · MOVPE

1 Introduction

InGaAs structures are one of the most significant III-V semiconductor materials and are widely used in various applications such as remote sensing, environmental monitoring, and fiber optic communication [1–3] due to their high electron mobility and large saturation shift speed. [4]. The InGaAs-based semiconductor devices have broad operation wavelengths ranging from 0.85 to 3.60 µm. [5]. Lattice-matched InP/InGaAs structure [6] has been broadly investigated for applications in short-wave infrared photodetectors [5, 7–10], transistors [1, 11, 12], and high-speed devices [13, 14]. In terms of the preparation technology of crystal materials, the InP substrate is less mature when compared to GaAs substrates. Moreover, InP, which is much more expensive than the same size GaAs wafer, has low mechanical strength and breaks easily. Although the InP substrate has the above disadvantages, it is theoretically more convenient as a base material due to its electrical properties and lattice mismatch [7, 15, 16]. For the above-mentioned reasons, InP substrates depicted promising performance in the range of 0.9–1.6 µm wavelength region for the potential applications from the photodetector to photodiodes, to name just a few [17–22]. For the above-mentioned properties and broad application areas, studying InP-based InGaAs structures is a perfect match to investigate more potential applications.

Various epitaxial growth technologies such as molecular beam epitaxy (MBE) [1, 23, 24], solid phase epitaxy (SPE) [1, 25], physical vapor deposition (PVD) [1, 26], and metal–organic vapor phase epitaxy (MOVPE) have been investigated to obtain promising semiconductor thin films. Among others, MOVPE has been in use for the preparation of $In_xGa_{1-x}As$ materials since 1968 [1, 27, 28]. One of the advantages of the MOVPE system is that high crystal quality layer can be obtained at a very high growth rate with multiple simultaneous growths. This advantage enables the MOVPE system suitable for mass production [29]. Growth parameters such as reactor pressure, substrate temperature, inlet source flow rate, alloy composition, and V/III ratio influence the properties of $In_xGa_{1-x}As$ epitaxial layers grown by MOVPE [30]. To control the quality of epitaxial layers, it is necessary to understand the effects of these parameters on the properties of the epitaxial layer

✉ Ilkay Demir
idemir@cumhuriyet.edu.tr

[1] Nanophotonics Research and Application Center, Sivas Cumhuriyet University, 58140 Sivas, Turkey

[2] Department of Nanotechnology Engineering, Sivas Cumhuriyet University, 58140 Sivas, Turkey

[14]. The variation of indium (In) concentration in the $In_xGa_{1-x}As$ alloy is important. For example, Smiri et al. [2] investigated the effect of different indium contents on crystal quality and optical properties and found that lattice mismatch increases at a higher In concentration. Likewise, the pit dislocation density increased with increasing indium concentration. Behcet et al. [29] investigated the structural and optical characterization of InGaAs samples with different indium concentrations. Indium concentrations were calculated with the HRXRD system, and the strain types of the films were determined. The optical properties of the films were measured by spectroscopic ellipsometry. As a result of spectroscopic ellipsometer measurements, they found that the refractive index values of the grown samples with almost the same indium concentrations were very close to each other and the refractive indices of the material increased with the increase of indium concentration. Asar et al. investigated the effects of indium alloy composition and metallization at room temperature on the structural and electrical properties of InGaAs/InP structures grown with MBE. The indium alloy composition of the structures was determined by HRXRD measurements, and indium homogeneity was determined by SIMS measurements, which were shown that the grown structures were of good crystal quality. In addition, the structure with the lowest FWHM value was closest to the lattice-matched InGaAs/InP structure. It is found that In concentration values obtained from HRXRD measurements agree with that of SIMS measurements [5].

The energy band gap of InGaAs structure is in the range of the infrared to the mid-infrared spectral region and makes InGaAs a suitable material for infrared device applications [29]. Therefore, energy band gap measurement is extremely important with desired properties such as optimum thickness, refractive index, optical reflection/transmission, and band gap seems to be essential. According to the above-mentioned properties of InP/InGaAs structure, the optimum structure parameters seem to be essential for promising detector technologies.

In this paper, we introduce a new experimental approach to controlling In concentration of InP/InGaAs structure while controlling the AsH_3 flow. The MOVPE system-grown InGaAs structures on InP substrates at different AsH_3 flows have been explored in terms of the structural and optical properties. This paper aims to understand the effects of In concentration on the structural and optical properties of InGaAs structure. This is important to know the effect of In content before integration into opto-electronic device applications. This article is formulated as: Sect. 2 gives the experimental approach. Section 3 explains the result and discussion, and Sect. 4, finally, shows the conclusion.

2 Material Method

The state-of-the-art crystal growth system (MOVPE) was used to growth of the InGaAs epilayers. All n-InGaAs epilayers were grown on indium phosphide (SI-InP) substrates. Trimethylgallium (TMGa) and trimethylindium (TMIn) were used as Ga and In precursors (group-III), respectively. High-purity (99.999%) arsine (AsH_3) and phosphine (PH_3) were used as As and P precursors (group-V) and silane (SiH_4) as n-type doping. Ultra-highly purified hydrogen (H_2) was used as carrier gas. We grew ~ 1000-nm-thick n-InGaAs epilayers with two different AsH_3 flows. The reactor temperature and pressure were set at 610 °C and 50 mbar, respectively. Figure 1 schematically represents the structure of n-InGaAs epilayers.

Uniform (thickness, composition, etc.) epitaxial layers were obtained using gas flow rotation. All flows and growth conditions were kept constant, but the AsH_3 flows used as the As precursor were changed to 80 and 110 sscm. Thus, the V/III ratio was changed from 118 to 162. The structural and optical characterizations have investigated the effects of different AsH_3 flow on the InGaAs epilayers.

In the structural characterization, the X-ray diffraction technique, which is inevitable for the non-destructive evaluation of crystalline materials, was used [31]. HRXRD measurements were taken by using Rigaku diffractometer. Spectroscopic ellipsometry (SE), a sensitive, precise, and non-destructive method, was used for the refractive indices and thickness analysis of InGaAs layers. Measurements were taken with the OPT-S9000 Spectroscopic Ellipsometer system in the range of 500–1650 nm at an angle of 65°. The reflection and energy band gap measurements of InGaAs heterostructures were performed by using Varian Cary 5000 UV–VIS–NIR Spectrophotometer system.

3 Results and Discussion

3.1 XRD Results

For the structural characterization of the $In_xGa_{1-x}As/InP$ sample, θ-2θ scanning was performed with the HR-XRD

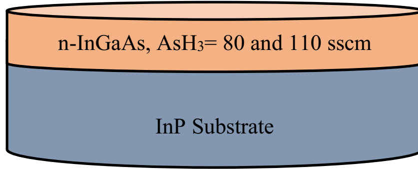

Fig. 1 Schematic representation of n-InGaAs epilayer growths by MOVPE

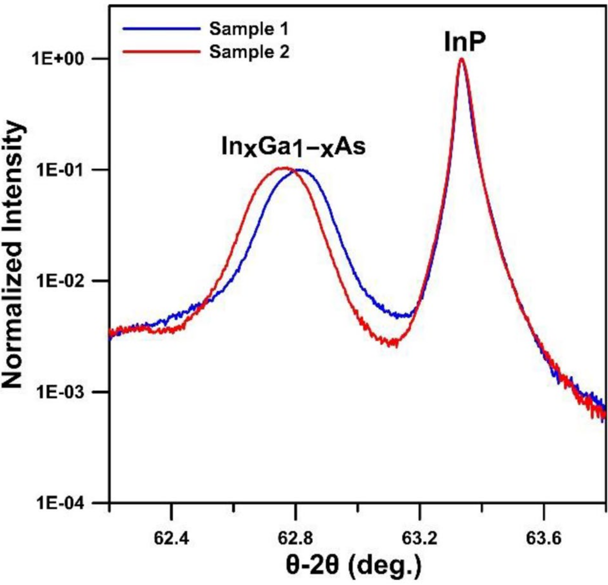

Fig. 2 θ-2θ scans of Sample 1 and Sample 2

technique, Fig. 2. With this technique, the crystal quality and alloy(x) ratios of the layers are determined.

In these scans, peak intensity and FWHM are related to crystal quality [32]. The FWHM value (Table 1) gives information about the stress occurring in the structure. High-intensity sharp peaks seen in Fig. 2 are derived from InP substrates, and other peaks are derived from $In_xGa_{1-x}As$ layers. The $In_xGa_{1-x}As$ peaks for all samples appear to the left of the InP peak. That means the film is under compression stress which results in an improvement in the out-of-plane lattice parameter. With the increment of AsH_3 flow (red line), the peak position left-shifted. The phenomena could be explained that as the AsH_3 flow increases, the Bragg peak shifts more toward the left side (low 2θ) angles. The reason behind this behavior is that the In concentration increases with the increment of AsH_3 flow, although the TMIn flow remains constant. increment of In concentration is attributed to surface kinetics, i.e., the V/III ratio increases, statistically more As atoms bind to Ga atoms due to weaker binding of In-As. In atoms combine with As atoms on the surface. If the V/III ratio is increased, the In atoms have a greater chance of bonding with As atoms due to this excess supply. Therefore, increasing AsH_3 flow results in extra As atoms available to combine In [33]. Using the HRXRD data, the In concentration was found to be 0.585 for Sample 1 and 0.59 for Sample 2. At the same time, the compression stress increases. From the XRD peak profile analysis, the crystallite size and peak broadening, and lattice stress due to dislocation are measured. [34].

Lattice parameters of InGaAs layer can be found by using Vegard's law [35].

$$a_{InGaAs} = (x)a_{InAs} + (1-x)a_{GaAs}. \quad (1)$$

The greater the mismatch between substrate and $In_xGa_{1-x}As$, the greater the full width of the Bragg peak at half maximum (FWHM). At the same time, dislocations occur. Based on the literature, the dislocation density in the grown epitaxial layers is calculated using the formula (N_{dis}) [36].

$$N_{dis} = 2\frac{(FWHM)^2}{9a_0^2}. \quad (2)$$

where a_0 is the lattice constant of the epitaxial layers found above from Vegard's law.

Then, the dislocation density of the samples is calculated using Eq. (2). All calculated values are given in Table 1. The half maximum (FWHM) value for constant film thickness is larger to release the mismatch stress exerted by the full width of the Bragg peak when the mismatch between InGaAs films and InP substrate is large [2]. The In concentration increases with the increment of AsH_3 flow, and the FWHM value also increases. The dislocation density calculated with the help of FWHM and lattice constant increases with the flow of AsH_3.

From this point of view, it is concluded that the crystal quality (CQ) of Sample 1 is slightly better than that of Sample 2 because it is closer to the lattice-compatible $In_{0.53}Ga_{0.47}As$/InP structure [5]. On the other hand, the FWHM values for two AsH_3 flow ratios are close (with a variation of %0.5), which could be negligible. Even though the calculation presents that the CQ of Sample 1 is better than that of Sample 2, the AsH_3 flow does not have an important effect on the structure properties. On the other hand, the effects of AsH_3 flow have a noticeable effect on the optical properties of the structures.

Table 1 The n-InGaAs epitaxial layers HR-XRD results in different AsH_3 flow

Sample	AsH_3 flow (sscm)	In content(%)	Lattice(Å)	FWHM (degree)	Dislocation density (10^9 cm^{-2})
1	80	58.7	5.891	0.195	3.155
2	110	59.2	5.893	0.196	3.185

3.2 Spectroscopic Ellipsometry Results

The refractive index values and thickness of the samples were obtained by using a spectroscopic ellipsometer. Ellipsometry yields correspond to the complex ratio ρ between Fresnel's reflection coefficients r_p and r_s [37]

$$\rho = \frac{r_p}{r_s} = \tan(\Psi)e^{i\Delta}. \tag{3}$$

where Ψ and Δ are ellipsometric parameters [38]. R_p and r_s represent complex Fresnel reflection coefficients for p- and s-polarized light, respectively [39].

The film thickness and refractive index values were obtained by fitting the experimental data. For the fitting, the Cauchy model has been used for the simulation since the Cauchy model is a simpler model requiring fewer parameters to determine the thickness and optical constants of semiconductor films. This model is suitable for materials with monotonically decreasing refractive index with increasing wavelength [40–43]. The Cauchy model formula is given [40]

$$n(\lambda) = A + \frac{B}{\lambda.^2} + \frac{C}{\lambda.^4}. \tag{4}$$

where A, B, and C are fit coefficients, and λ is the wavelength in nanometers.

Figures 3 and 4 show Δ and Ψ measurements (solid line) and fits (dashed line) for Sample 1 and Sample 2. It is seen that the simulation and experimental measurements are in agreement. Light incident on a thin film is reflected by both the upper and lower interfaces. Each reflected wave will have its phase and amplitude causing interference from the reflected light. As can be seen from Figs. 3 and 4, thicker films will show more interference fringes [44]. These fringes are very close to each other because the thicknesses of the grown samples are also very close. As a result of the simulation, the thin film thicknesses for Sample 1 and Sample 2 were determined as 1025 nm and 1027 nm, respectively. These values are in agreement with the growth thickness calculated by MOVPE with deviations of 2.5% and 2.7% for Sample 1 and Sample 2, respectively. The predicted refractive indices were used in determining the thickness with the in situ measurement system during growth due to the uncertainty of the indium concentration of the $In_xGa_{1-x}As$ layers. These could be the cause of these small deviations.

The spectroscopic ellipsometry measurement of two samples at different AsH_3 flows and the refractive index graph obtained as a result of the fit are given in Fig. 5.

The increment of the AsH_3 flow leads to the increment of the indium concentration due to weaker bonding of In-As. Theoretical studies for determining the refractive index values of InGaAs structure have been reported in the literature [29]. As shown in Fig. 5, the refractive index of Sample 2 is larger than Sample 1. Although there are several studies on the characterization of InP/InGaAs structure, optimum structure parameters with desired properties are necessary for obtaining IR and mid-IR detector structures, i.e., optimum optical transmission and the energy band gap.

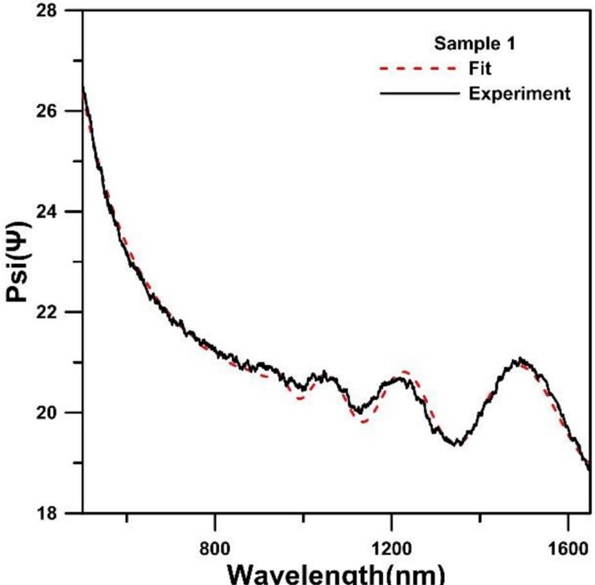

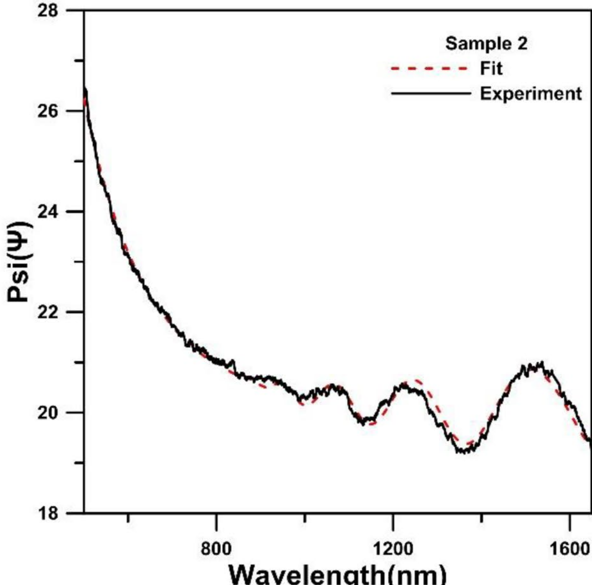

Fig. 3 Experimental (the black solid line) and simulation (the red dashed line) results for spectroscopic ellipsometry parameter (Ψ) of Sample 1 and Sample 2

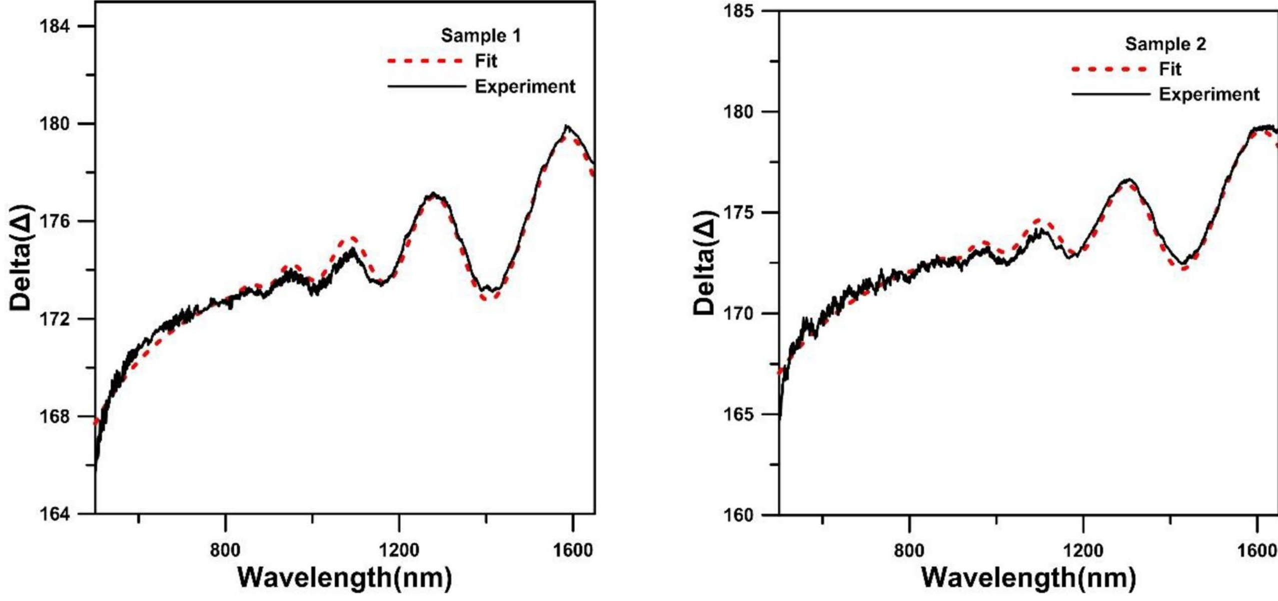

Fig. 4 Experimental (the black solid line) and simulation (the red dashed line) results for spectroscopic ellipsometry parameter (Δ) of Sample 1 and Sample 2

3.3 UV–VIS–NIR Spectrophotometer Results

Total reflectance spectra were measured by a Varian spectrophotometer in the range of 800–2300 nm at room temperature. The total reflection spectra were measured in the range of 800–2300 nm at room temperature. The total reflection graph for Sample 1 and Sample 2 is given in Fig. 6.

The ratio of the reflected energies to the incident energies and the capability to reflect the energy event on the surface of a material is called reflection (R) [45]. The amount of reflected light and its reflection direction

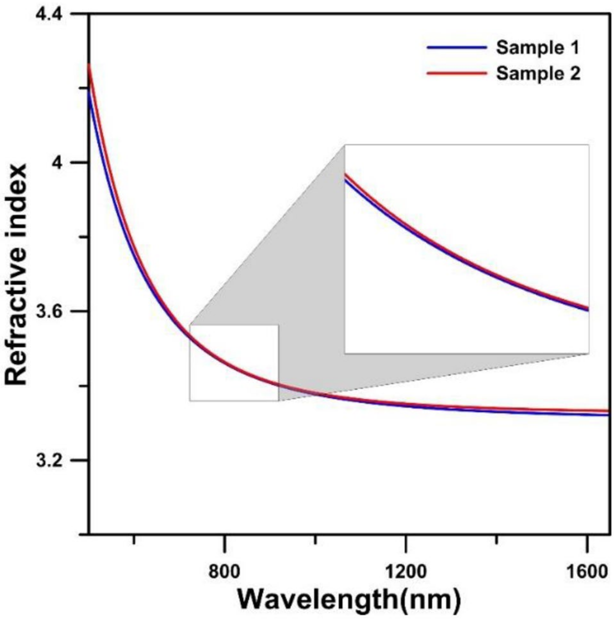

Fig. 5 Refractive index values as a function of wavelengths for $In_xGa_{1-x}As$ films

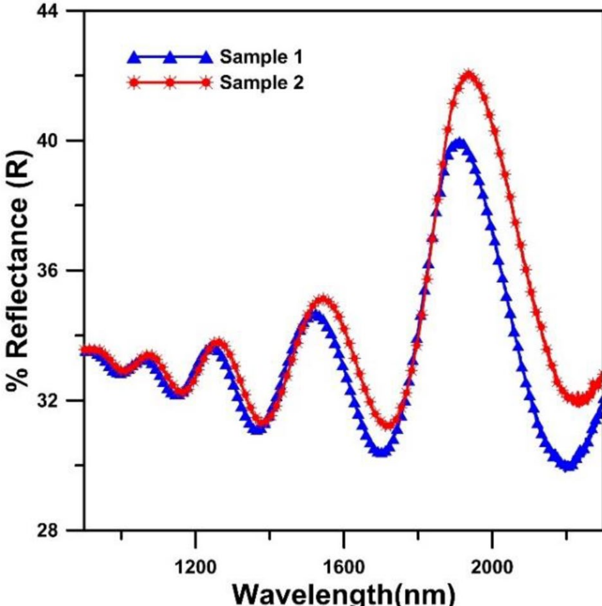

Fig. 6 Total reflectance versus wavelength(nm) of Sample 1 and Sample 2

Springer

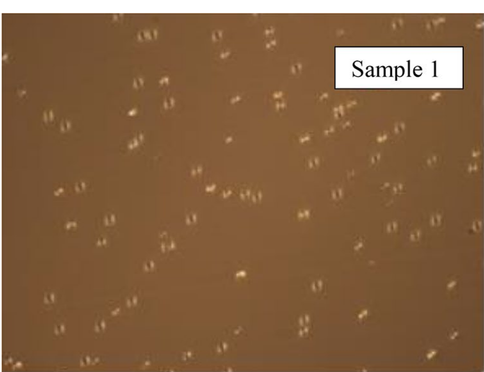

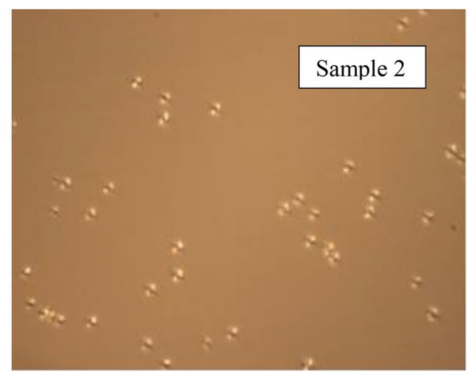

Fig. 7 Optical microscope image of Sample 1 and Sample 2

depends on the surface texture. Almost all light is reflected equally when surface defects are smaller than the wavelength of incident light [46]. The variation of reflection seen in Fig. 6 is attributed to the surfaces of the film obtained with an optical microscope, Fig. 7. Thin-film surface improves at high AsH_3 flow, Fig. 7(b). The increment in the total reflection at high AsH_3 flow (Fig. 6) is related to the improvement of the sample surface [47]. As desorption from a grown structure results in surface degradation. To prevent this drawback, increasing the V/III ratio by increasing AsH_3 flow, restores the surface desorption [33]. For this reason, high V/III ratios are required to obtain good surface morphology [48].

The diffuse reflection spectra were measured in the range of 800–2300 nm at room temperature. Using the diffuse reflection of the sample, the Kubelka–Munk function F(R) was obtained. This formula is given [47, 48]

$$F(R) = \frac{(1-R)^2}{2R}. \tag{5}$$

where R represents the diffuse reflectance values of the samples. The energy band gaps of the films are found using the Kubelka–Munk function. $(F(R)E/d)^2$ as a function of the energy graph is shown in Fig. 8, where d is the thickness of the thin films determined by the spectroscopic ellipsometer.

The energy band gap of the films is determined from Fig. 8. The intersection point of the tangents line of the linear portion of the graph with the x-axis (energy) gives the band gap of the structure, and slope lines (the black solid line) are added from the linear part of the graph to the x-axis. The energy band gap was found to be 0.630 eV for Sample 1 and 0.6190 eV for Sample 2.

The increment of the AsH_3 flow increases the In concentration, which decreases the energy band gap of the material because the energy band gap approaches InAs.

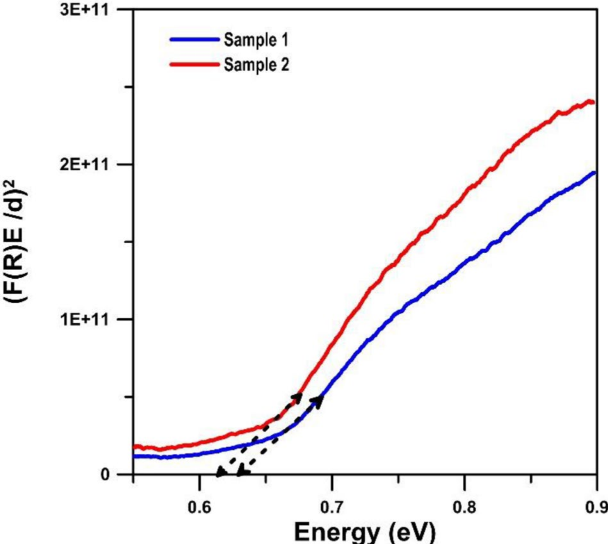

Fig. 8 $(F(R)E/d)^2$) versus photon energy (eV) of Sample 1 and Sample 2

4 Conclusion

In this paper, we have investigated the structural and optical properties of MOVPE-grown InGaAs structures on the InP substrate. The characterizations of these structures have been investigated as a function of the AsH_3 flows. The crystal quality and In concentrations of the samples were determined with the HRXRD system. From these results, it was observed that the In concentrations of the samples changed with the increase of AsH_3 flow, although the TMIn flow remained constant. The reason for this result can be explained as follows. Although the tendency of As to combine with Ga is still high due to the weak binding of In-As, the chance of In atoms bonding with As atoms are higher due to this excess supply. Therefore, increasing the AsH_3 flow results in extra As atoms available to combine In. From the HRXRD results, it was observed that the increase of AsH_3 flow affected the In concentration, but did not change the crystal quality much. With the calculations, it was seen that the difference in crystal quality between the two samples could be

ignored. However, the effects of AsH_3 flow have a noticeable effect on the optical properties of the structures. The optical properties of the grown epitaxial layers were determined with the spectroscopic ellipsometer and spectrophotometer. The refractive indices and thicknesses of the films were primarily determined by spectroscopic ellipsometry. Increasing In concentration with increasing AsH_3 flow increased the refractive indices of the epitaxial layers. The determined thicknesses were obtained to be 2.5–2.7% higher than those determined in the MOVPE system. The optical reflection and band gaps of the films were determined by the spectrophotometer system. The increased AsH_3 flow improves the surface quality of the structure and total reflectance increases. This is attributed to the increment of As flow improves the surface texture. Finally, the energy band gaps of the films decreased with increasing AsH_3 flow, which caused an increase in the In concentration. In addition, the energy band gap of the structure approaches InAs having a lower energy band gap.

Acknowledgements This work is supported by the Scientific Research Project Fund of Sivas Cumhuriyet University under the project number [M-2021-821].

Funding This work is supported by the Scientific Research Project Fund of Sivas Cumhuriyet University under the project number [M-2021–821].

Declarations

Conflicts of Interest The authors declare no competing interests.

References

1. L. Zhao, Z. Guo, Q. Wei, Q. Miao, L. Zhao, Sci. Rep. **6**, 1 (2016)
2. B. Smiri, M.B. Arbia, I. Demir, F. Saidi, Z. Othmen, B. Dkhil, H. Maaref, Mater. Sci. Eng., B **262**, 114769 (2020)
3. D.N. Buckley, J. Electron. Mater. **17**, 15 (1988)
4. T.W. Nee, A.K. Green, J. Appl. Phys. **68**, 5314 (1990)
5. T. Asar, S. Özçelik, E. Özbay, J. Appl. Phys. **115**, 104502 (2014)
6. D.K. Gaskill, N. Bottka, L. Aina, Appl. Phys. Lett. **56**, 1269 (1990)
7. L. Zhao, Z. Guo, M. Zhang, S. Yang, L. Zhao, Surf. Interface Anal. **51**, 498 (2019)
8. J. Ma, Z. Zhang, G. Miao, Y. Zhao, Jpn. J. Appl. Phys. **54**, 104301 (2015)
9. J. Zhang, M.A. Itzler, H. Zbinden, J.W. Pan, Light Sci. Appl. **4**, 286 (2015)
10. L. Dou, Y.M. Yang, J. You, Z. Hong, W.H. Chang, G. Li, Y. Yang, Nat. Commun. **5**, 1 (2014)
11. J.A. Del Alamo, Nature **479**, 317 (2011)
12. C.L. Tsai, K.Y. Cheng, S.T. Chou, S.Y. Lin, C. Xu, K.C. Hsieh, J. Vac. Sci. Technol. B Microelectron. Nanometer Struct. Proc. Meas. Phenom. **26**, 1140 (2008)
13. L. Jiang, T. Lin, X. Wei, G.H. Wang, G.Z. Zhang, H.B. Zhang, X.Y. Ma, J. Cryst. Growth **260**, 23 (2004)
14. J.B. Yoo, J.S. Kim, D.H. Jang, B.H. Koak, D.K. Oh, H.M. Kim, Y.T. Lee, J. Cryst. Growth **132**, 43 (1993)
15. R. Deki, T. Sasaki, M. Takahasi, J. Cryst. Growth **468**, 241 (2017)
16. G.P. Dimitrakopulos, C. Bazioti, J. Grym, P. Gladkov, E. Hulicius, J. Pangrác, P. Komninou, Appl. Surf. Sci. **306**, 89 (2014)
17. J.J. Eckl, K.U. Schreiber, T. Schüler, Int. Soc. Opt. Photonics **10229** (2017)
18. J. Ma, B. Bai, L.J. Wang, C.Z. Tong, G. Jin, J. Zhang, J.W. Pan, Appl. Opt. **55**, 7497 (2016)
19. S. Cova, M. Ghioni, M.A. Itzler, J.C. Bienfang, A. Restelli, In Experimental Methods in the Physical Sciences **45**, 83 (2013)
20. A. Tosi, F. Acerbi, A. Dalla Mora, M.A. Itzler, X. Jiang, IEEE Phot. J. **3**, 31 (2010)
21. M.A. Itzler, X. Jiang, M. Entwistle, K. Slomkowski, A. Tosi, F. Acerbi, S. Cova, J. Mod. Opt. **58**, 174 (2011)
22. X. Jiang, M.A. Itzler, R. Ben-Michael, K. Slomkowski, IEEE J. Sel. Top. Quantum Electron. **13**, 895 (2007)
23. F. Gao, L. Wen, J. Li, Y. Guan, S. Zhang, G. Li, CrystEngComm **16**, 10774 (2014)
24. Z.Y. Zhang, A.E. Oehler, B. Resan, S. Kurmulis, K.J. Zhou, Q. Wang, R.A. Hogg, Sci. Rep. **2**, 1 (2012)
25. I. Suzumura, M. Okada, A. Muto, Y. Torige, H. Ikeda, A. Sakai, Y. Yasuda, Thin Solid Films **369**, 116 (2000)
26. T. Speliotis, E. Makarona, F. Chouliaras, C. A. Charitidis, C. Tsamis, D. Niarchos, Phys. Status Solidi C **5**, 3759 (2008)
27. H.M. Manasevit, Appl. Phys. Lett. **12**, 156 (1968)
28. C.D. Wood, O. Hatem, J.E. Cunningham, E.H. Linfield, A.G. Davies, P.J. Cannard, D.G. Moodie, Appl. Phys. Lett. **96**, 194104 (2010)
29. B.O. Alaydın, E.S. Tüzemen, I. Demir, S. Elagöz, Cumhuriyet Sci. J. **38**, 681 (2017)
30. S. Elagöz, I. Demir, Gazi Univ. J. Sci. **29**, 947 (2016)
31. I. Demir, S. Elagoz, Superlattices Microstruct. **100**, 723 (2016)
32. I. Perkitel, I. Altuntaş, I. Demir, Gazi, The effect of Si (111) Substrate surface cleaning on growth rate and crystal quality of MOVPE Grown AlN . Gazi Univ. J. Sci. **35** (1), 281-291 (2022). https://doi.org/10.35378/gujs.822954
33. J. Dharma, A. Pisal, C.T. Shelton, Appl. Note (2009)
34. P. Bindu, S. Thomas, J. Theor. Appl. Phys. **8**, 123 (2014)
35. D. Zhou, B.F. Usher, J. Phys. D Appl. Phys. **34**, 1461 (2001)
36. S.Z. Chang, T.C. Chang, L.J. Shen, S.C. Lee, Y.F. Chen, J. Appl. Phys. **74**, 6912 (1993)
37. Z.H. Dai, R.J. Zhang, J. Shao, Y.M. Chen, Y.X. Zheng, J.D. Wu, L.Y. Chen, J. Korean Phys. Soc. **55**, 1227 (2009)
38. D.E. Morton, B. Johs, J. Hale, in *Proceedings of the annual technical conference-society of vacuum coaters.* (2002), p. 299
39. R. Pascu, M. Dinescu, Romanian Rep. Phys. **64**, 135 (2012)
40. R.A. Synowicki, Thin Solid Films **313**, 394–397 (1998)
41. D. Shah, D.I. Patel, N.H. James, M.R. Linford, Vacu. Technol. Coating 29–33 (2019)
42. O. Gençyilmaz, F. Atay, IS. Akyüz, Süleyman Demirel Üniversitesi Fen Edebiyat Fakültesi Fen Dergisi **9**(2), 137–146 (2014)
43. https://www.horiba.com/int/scientific/technologies/spectroscopic-ellipsometry/cauchy-dispersion-module/. Accessed 7 July 2022
44. https://www.eag.com/wp-content/uploads/2020/04/M-040242-Spectroscopic-Ellipsometry_web.pdf. Accessed 17 Apr 2020
45. H. Aydin, B. Gündüz, C. Aydin, Synth. Met. **252**, 1 (2019)
46. https://www.olympus-lifescience.com/en/microscope-resource/primer/lightandcolor/reflectionintro/. Accessed 9 Nov 2021
47. E.S. Tuzemen, S. Elagoz, H. Sahin, K. Kara, R. Esen, A. Bulut, Marmara Fen Bilimleri Dergisi **25**, 41 (2013)
48. C.P. Kuo, R.M. Cohen, K.L. Fry, G.B. Stringfellow, J. Electron. Mater. **14**, 231 (1985)

Publisher's Note Springer Nature remains neutral with regard to jurisdictional claims in published maps and institutional affiliations.

Springer Nature or its licensor holds exclusive rights to this article under a publishing agreement with the author(s) or other rightsholder(s); author self-archiving of the accepted manuscript version of this article is solely governed by the terms of such publishing agreement and applicable law.